Proc. Natl. Acad. Sci. USA
Vol. 84, pp. 5511–5515, August 1987
Chemistry

Simulation of photochemical hole-burning experiments on photosynthetic reaction centers

(photosynthetic electron transfer/vibronic coupling theory)

YOUNGDO WON AND RICHARD A. FRIESNER

Department of Chemistry, The University of Texas at Austin, Austin, TX 78712-1167

Communicated by Allen J. Bard, April 20, 1987 (received for review August 20, 1986)

ABSTRACT **An effective Hamiltonian formalism is used to calculate the homogeneous linewidth of long-wavelength absorption in the photosynthetic reaction center. Agreement with the experimental values of ≈400 cm^{-1} for the hole width of the 990-nm band of *Rhodopseudomonas viridis* is obtained. The anomalously (two orders of magnitude) large width is explained in terms of resonant coupling to charge transfer states. These results support a dynamical model of primary charge separation [Friesner, R. & Wertheimer, R. (1982) *Proc. Natl. Acad. Sci USA* 79, 2138–2142] in which such resonant coupling was also concluded to be important.**

The elucidation of the crystal structure of reaction centers from *Rhodopseudomonas viridis* by Deisenhofer and coworkers (1) has inaugurated a new era in the study of the photosynthetic light reactions. Instead of focusing on the identity and geometrical arrangements of reaction center components, one can now try to understand the interactions between components and the consequent dynamics. Unfortunately, the relevant parameters cannot, in the absence of a reliable electronic structure method, be quantitatively determined from the x-ray coordinates in a straightforward fashion. Therefore, it is necessary to construct effective Hamiltonian models and test these by comparison with experiment.

In the present letter, we employ a model very similar to one used previously in simulation of primary charge separation in the reaction center (2). We show that the model provides a simple explanation of the striking qualitative aspects of the results obtained by Boxer and coworkers (3, 4) and Meech *et al.* (5) from photochemical hole-burning experiments. In a subsequent paper, agreement for various other optical properties (linear dichroism, circular dichroism) will also be demonstrated. While the large number of energy parameters and possible terms in the Hamiltonian preclude a definitive analysis, the present theoretical approach does provide a consistent, unified picture of the spectroscopy and dynamics of the reaction center.

The essence of the experimental observations of Boxer and coworkers is as follows. In both the photosynthetic bacteria *Rps. viridis* and *Rhodobacter sphaeroides*, a hole width of roughly 400 cm^{-1} (80–95% of the width measured by conventional absorption experiments) is observed at 1.5 K for the low-energy absorption band associated with the primary donor. This result, which is relatively temperature independent and insensitive to excitation wavelength, is to be contrasted to the widths of a few hundredths of wavenumbers observed for, e.g., chlorin in glassy media by Völker and Macfarlane (6). Recent experiments indicate that hole widths of similar magnitude are also observed when a chlorophyll is inserted into myoglobin (25) so that the generic features of the protein environment are unlikely to be responsible for the four-orders-of-magnitude discrepancy.

An important aspect of our calculations is the explicit inclusion of vibronic coupling terms in the Hamiltonian. This inclusion is essential in understanding the mechanism by which the anomalously large hole width described above is produced. We argue that our analysis of the experiment supports the suggestion in ref. 2 of resonant coupling between excited states of the primary donor and charge-separated vibronic levels.

MODEL

We will be concerned with the long-wavelength (≈990-nm) absorption band of reaction centers from *Rps. viridis*. The principal contribution of oscillator strength in this region is clearly the special pair (SP) bacteriochlorophyll (BChl) dimer Q_y transition. However, the admixture of other electronic states must also be considered.

The reaction center contains a large number of components that can exist in a variety of possible electronic configurations. To construct the simplest effective Hamiltonian that is capable of addressing the experiments considered here, we adopt the following strategy. Only those electronic states postulated to contain vibronic levels that are strongly coupled to and nearly resonant with the 990-nm SP Q_y exciton component (henceforth designated relevant states) are included explicitly in the Hamiltonian. The remaining states and the protein environment are assumed to perturbatively interact with the relevant states, renormalizing their diagonal energies, interactions, and oscillator strengths; the parameters that appear in Eq. 1 are to be interpreted as these renormalized parameters. This approach in fact entails the standard justification for effective Hamiltonians in, e.g., solid-state physics applications.

Assumptions must then be made concerning which states are to be included in the relevant set. Many states that have been proposed to affect the Q_y absorption spectrum [e.g., the Q_x states of various chromophores (7)] are sufficiently well separated in energy that a perturbative treatment is acceptable, and the arguments of the previous paragraph can be applied. This does not mean that such states are not important in a first-principles calculation of reaction center optical spectra, but rather that all such effects are incorporated into our Hamiltonian phenomenologically, independent of origin. For example, our calculations are agnostic on the source of the red shift of the SP Q_y band; this question can be addressed theoretically only by electronic structure calculations. We simply adjust the SP site energies so that the experimental result is reproduced.

The central hypothesis of this paper (presented earlier in ref. 2) is that the charge transfer (CT) configurations that participate in the initial stages of the photosynthetic light reactions are resonantly coupled to the initial SP 990-nm excited state. As experimental evidence indicates that charge separation proceeds primarily through only one side of the sym-

The publication costs of this article were defrayed in part by page charge payment. This article must therefore be hereby marked "*advertisement*" in accordance with 18 U.S.C. §1734 solely to indicate this fact.

Abbreviations: SP, special pair; CT, charge transfer; BChl or B, bacteriochlorophyll; H, bacteriopheophytin; P, primary electron donor.

metrically branched arrangement of the BChl and bacteriopheophytin (BPh) chromophores in the reaction centers (8), we include just one proximate BChl (designated B) and one BPh (H) in our model. Presumably, CT configurations involving these molecules are electrostatically stabilized by the protein environment, whereas CT configurations involving the remaining chromophores remain at high energy and interact perturbatively.

Recent femtosecond experiments (9) cast substantial doubt on whether the state P^+B^- (as one would conventionally interpret it, with P representing the primary electron donor) is actually an intermediate in the initial charge separation. An alternative that has been suggested is participation of an internal charge-separated state of the dimer (10). The present calculations do not directly address the issue of the precise sequence of electronic states that are involved. As there are still a number of possible explanations, we retain the notation of ref. 2, with the understanding that the intermediate CT state designated here by P^+B^- may in fact have a different electronic character.

On the basis of the above discussion, six electronic states are included in our excited state manifold. They are (in order of labeling) $P_1^*P_2BH$, $P_1P_2^*BH$, $P_1^+P_2B^-H$, $P_1P_2^+B^-H$, $P_1^+P_2BH^-$, and $P_1P_2^+BH^-$. Here P_1 is the SP BChl closest to B, and P_2 is the most distant. The interactions between these zeroth-order states reside in a 6×6 matrix ε. Table 1 relates the elements of ε to the physical parameters J (SP exchange interaction), J_R (CT exchange interaction, due to the existence of two dimeric states for each CT configuration), K (P^+B^-H–P^+BH^- exchange interaction), Δ_{PH} (P^*BH–P^+BH^- energy gap), Δ_{BH} (P^+B^-H–P^+BH^- energy gap), and J_{CT} (P^*–P^+B^- exchange interaction). The notation adopted is that of ref. 2. The electronic parameter values are estimated as described in ref. 2; the actual numerical values used here have been modified to be consistent with the *Rps. viridis* experimental data.

The vibrational modes most strongly coupled to the 990-nm optical transition will be those associated with the SP molecules. Unfortunately, no highly resolved absorption spectra of the Q_y transition of BChl are presently available. Construction of our theoretical model would be greatly facilitated by such experiments, although uncertainties concerning interaction with the protein environment would still remain.

Six intramolecular modes (one set for each SP monomer, yielding 12 modes in all) are extracted from the site selection spectrum of chlorophyll *a* obtained by Platenkamp *et al.* (12); in some cases, two closely spaced frequencies are combined into a single mode. The resulting molecular vibrational modes have frequencies of 140, 260, 348, 388, 479, and 569 cm^{-1}. Inclusion of additional high-frequency modes (>750 cm^{-1}) has little effect on our results, as would modes on the B or H molecules.

Direct determination of vibronic coupling constants from the data of ref. 12 is not possible because the intensity of the zero-phonon line is not accurately measured in the site selection experiments. Consequently, we first compute the coupling parameter for the 140 cm^{-1} mode from the supersonic jet spectrum of free-base porphin obtained by Even *et al.* (13), then scale the site selection spectrum to this value to obtain the remaining coupling constants. The corresponding vibronic coupling parameters of the six intramolecular modes are 64.6, 94.3, 149.4, 132.6, 116.8, and 116.2 cm^{-1}.

Table 1. Electronic parameters for the effective Hamiltonian

Parameter	Value, cm^{-1}
ε_{11}	11,045.0
Δ_{PH}	600.0
Δ_{BH}	200.0*
J	872.0
J_R	612.0
J_{CT}	240.0
K	14.6

$\varepsilon_{55} = \varepsilon_{66} = \varepsilon_{11} - J + J_R - \Delta_{PH}$; $\varepsilon_{33} = \varepsilon_{44} = \varepsilon_{55} + \Delta_{BH}$; $\varepsilon_{12} = \varepsilon_{21} = J$, $\varepsilon_{34} = \varepsilon_{43} = \varepsilon_{56} = \varepsilon_{65} = J_R$, and $\varepsilon_{13} = \varepsilon_{31} = J_{CT}$; $\varepsilon_{35} = \varepsilon_{46} = \varepsilon_{53} = \varepsilon_{64} = K$. All other values are 0 and the ε matrix is symmetric.
*From ref. 11.

The site selection spectra of ref. 12 also display several strongly coupled librational modes in the 100-cm^{-1} frequency region. We include one effective librational mode of 117 cm^{-1} in our model, with a coupling constant, 50.6 cm^{-1}, estimated from the scaled site selection absorption intensities. In view of the fact that both the n-C_8 matrix employed in ref. 12 and the reaction center protein are relatively rigid, nonpolar media, this procedure appears reasonable.

A final discrete mode likely to be of importance is the intermolecular relative motion of the SP molecules, which strongly modulate the exchange interaction. This effect is manifested in the Hamiltonian as an off-diagonal coupling matrix element. A vibrational frequency of 50 cm^{-1} is utilized. The coupling constant is treated as an adjustable parameter and set to 50 cm^{-1}.

All of the above modes can be expected to undergo a rather large change in equilibrium geometry upon production of a CT state. What is important for our purposes is the magnitude of this change, rather than the precise CT potential surfaces (the details of which have little effect on the 990-nm region optical lineshapes). Consequently, we estimate an average scale factor of 3 from Warshel's QCFF-PI calculations (14) for the CT vibronic coupling parameters as compared to the excited state coupling parameters (i.e., the former are roughly 3 times larger than the latter). Each value obtained above is thus multiplied by three to give the corresponding value in CT state.

Two medium effects are phenomenologically included in the Hamiltonian: coupling to acoustic phonons and inhomogeneous broadening. In accordance with the nonphotochemical hole burning results cited above, we expect the acoustic phonons to make negligible contribution to the homogeneous linewidth at low temperatures; a Lorentzian damping factor of 1 cm^{-1} is utilized in the calculation for numerical convenience. Inhomogeneous broadening is incorporated by convoluting the homogeneous lineshapes with a Gaussian function representing a distribution of SP site energies. The Gaussian linewidth parameter is adjusted to reproduce the low-temperature absorption spectra in the 990-nm region.

THEORY

The effective Hamiltonian for the excited state manifold described in the preceding section can be written in second quantized form as

$$\mathscr{H} = \sum_{ij=1}^{6} |i\rangle\langle j|\varepsilon_{ij} + \sum_{n=1}^{14} \omega_n b_n^\dagger b_n + \sum_{ij}^{6}\sum_{n=1}^{14} \theta_{ij}^{(n)}|i\rangle\langle j|(b_n + b_n^\dagger). \quad [1]$$

Here the ε_{ij} are electronic coupling parameters, ω_n are vibrational frequencies, and the $\theta_{ij}^{(n)}$ are vibronic coupling parameters. We consider only linear vibronic coupling (i.e., shifts of the equilibrium geometry upon change of electronic state), which provides the dominant contribution to the vibronic mixing and level distributions. The operators b and $b^\dagger$ are the usual boson annihilation and creation operators, while $|i\rangle\langle j|$ is a projection operator connecting electronic state i to state j. The electronic ground state is assumed to be a single harmonic surface with unaltered frequencies ω_n. The calculation of all the parameter values has been detailed in the preceding section. Fourteen vibrational modes are included: six intramolecular modes on each SP monomer, one librational mode, and one intermolecular vibration mode, with frequencies given above. For the intramolecular and librational modes, θ is diagonal in the electronic state index—i.e., the vibration is a local one. For the intermolecular mode, the only nonzero elements are those that couple the two SP molecules (whether in the excited or CT state). The nonzero values of the appropriate $\theta_{ij}^{(n)}$ elements are just the linear vibronic coupling matrix elements determined in the preceding section from the site selection and supersonic jet experiments.

The absorption spectrum due to the Hamiltonian given in Eq. **1** cannot be obtained exactly, as there are a large number of degrees of freedom and no closed form analytic solutions exist. Therefore, we utilize an approximate Green's function approach (15), which has been extensively tested against converged basis set calculations for smaller analogous models (16). While precise peak heights are not always quantitatively rendered at high resolution, the overall intensity distribution and degree of spectral congestion are reproduced reasonably well in most cases. This level of computational reliability should be sufficient to address the questions of interest here. However, the approximations inherent in the method can be checked by performing ultralarge basis set calculations ($\approx 10^5$ quantum states) using the recursive residue generation method (17, 18).

Once the Green's function matrix elements $\mathbf{G}_{ij}(E)$ are obtained, the optical absorption is evaluated (in terms of intensity, I) from knowledge of the transitional dipole moments μ_i via the formula

$$I(E) = -\frac{1}{\pi} \sum_i \sum_j \vec{\mu}_i \cdot \vec{\mu}_j \, \mathrm{Im}\, \mathbf{G}_{ij}(E). \qquad [2]$$

We assume that only the SP molecules possess oscillator strength in this wavelength region, and we obtain the appropriate transition dipole vectors from the x-ray crystal coordinates (1). The monomer Q_y transition dipoles are taken to be along the axis running from the N atom of ring I to the N atom of ring III of the monomer (19).

RESULTS

We first calculate the 10-K absorption spectrum in the 990-nm region, adjusting the inhomogeneous broadening to reproduce the experimental results of Breton (20) (see Fig. 1). A value of 318 cm^{-1} (full width at half maximum of the Gaussian distribution function) is obtained for the Gaussian width parameter. Simulations of the remaining spectral region, as well as other optical properties, also yield acceptable results, as will be shown in a subsequent paper. The broad, featureless lineshape of Fig. 1 is (roughly) unaffected by the value of J_{CT}.

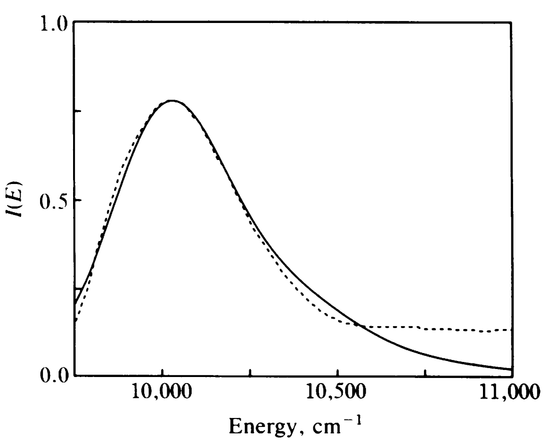

FIG. 1. Comparison of the 10-K absorption lineshape in the 990-nm region calculated from Eq. **1** (solid line) with the experimental results of Breton (broken line) (20). The vibronic coupling and electronic parameters are those given in Table 1 and *Model*. Inhomogeneous broadening is included via convolution over a Gaussian distribution with a full width at half-maximum of 318 cm^{-1}.

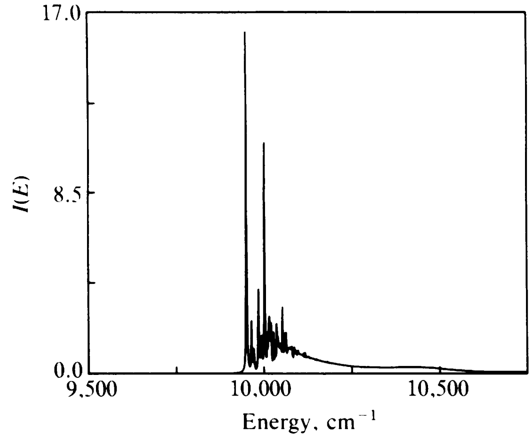

FIG. 2. Homogeneous absorption lineshape of the isolated SP manifold. All parameters are as in Fig. 1, except J_{CT} = 0 and no Gaussian broadening is incorporated.

We next set the inhomogeneous broadening equal to zero by eliminating the Gaussian convolution. Fig. 2 displays the homogeneous lineshape with J_{CT} set equal to zero. A strong zero-phonon line is present, followed by a progression of Franck–Condon peaks due to molecular vibrations. This computation predicts that a narrow hole would be observed if the SP dimer could be decoupled from the rest of the electron transfer system.

Fig. 3 displays the homogeneous lineshape obtained when J_{CT} is set equal to 240 cm^{-1}. A broad profile without sharp features is generated due to the strong interaction of the SP vibronic states with the CT manifolds. As J_{CT} is varied from 0 to 240 cm^{-1}, the zero-phonon line is gradually eliminated. Small variation of Δ_{PH} has little effect; a larger perturbation, moving the CT state out of resonance, again restores the zero-phonon line. The quantitative details of these observations will be presented elsewhere.

To compare our results directly with the experiments of refs. 3 and 4, we must calculate the absorption spectrum of the system after irradiation with a burn laser under appropriate experimental conditions. With the homogeneous line-

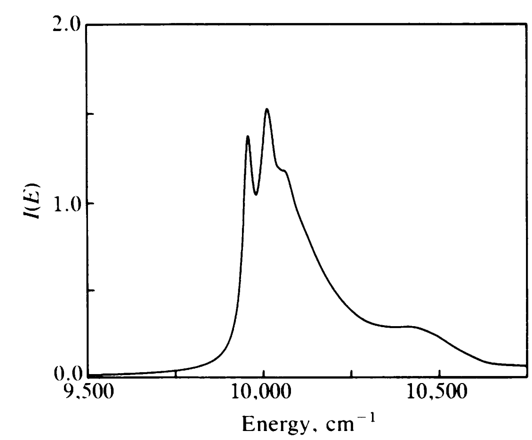

FIG. 3. Homogeneous absorption lineshape of the fully interacting chromophore system. All parameters are as in Fig. 2, except J_{CT} = 240 cm^{-1}.

shapes, $I_H(E)$, available, this is readily accomplished via an expression of Friedrich and Haarer (21):

$$I_t(E) = \int_{-\infty}^{\infty} \rho_I(E' - E_0) \exp[CI_H(E_L - E')]I_H(E - E')\, dE'. \quad [3]$$

Here ρ_I is the inhomogeneous distribution, E_0 the center of that distribution, $\omega_L = E_L/\hbar$ the frequency of the burn laser, I_H the homogeneous lineshape, and C a constant that depends on the absorption cross section σ, burn time t, a photon flux $\phi = I/\hbar\omega_L$, and photochemical quantum yield Φ—i.e.,

$$C = \frac{\sigma I}{\hbar\omega_L} \Phi t.$$

We have extracted an initial estimate of C from the experimental conditions described in refs. 3 and 4, then adjusted it so that the integrated depletion of the absorption spectrum corresponds to that measured in ref. 4 (approximately 7%).

Fig. 4 displays the spectrum predicted after irradiation at $\omega_L = 10{,}009$ cm^{-1}, with the CT resonance coupling turned off, $J_{CT} = 0$. The spectrum for C = 0 is reproduced for comparison. As expected, a narrow sharp zero-phonon hole (as well as several side holes) is observed. On the other hand, the results in Fig. 5 ($J_{CT} = 240$ cm^{-1}) reveal no such feature. This qualitative result remains true as ω_L is tuned across the absorption band, and it is insensitive to the precise values of molecular, librational, and intermolecular vibronic coupling constants. That is, strong, quasiresonant coupling to a CT manifold is necessary and sufficient to destroy the narrow zero-phonon hole observed in usual photochemical hole-burning experiments with organic glasses.

Fig. 6 presents the difference spectrum, $\Delta I_t = I_t - I_{t=0}$, for $J_{CT} = 240$ cm^{-1}. The width is about 350 cm^{-1}, in good agreement with experiment. The precise value of this width (as well as variation with ω_L) does depend on details of the Hamiltonian. Here we draw only the crude (but definite) conclusion that sufficiently strong coupling to low-frequency modes is required to achieve the observed hole width; if the librational and intermolecular coupling values were set equal to zero, a considerably smaller (about 150 cm^{-1}) width would result. Reliable identification of the relative contributions of various physical processes to this coupling will probably require additional experiments; the model used here is plausible but by no means the only one possible.

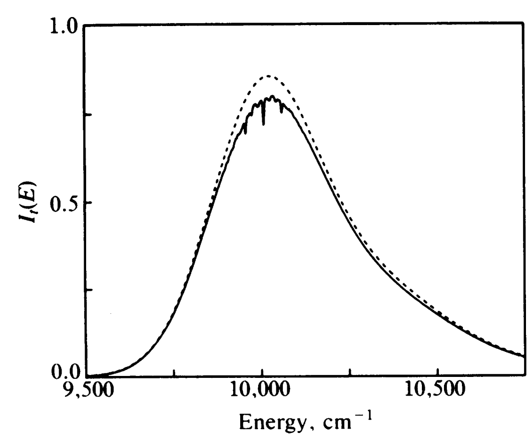

FIG. 4. Photochemically modified absorption spectrum for the isolated SP system (solid line, $J_{CT} = 0$) calculated by using Eq. 3. $C = 0.07$ and $\omega_L = 10{,}009$ cm^{-1}. The spectrum with $C = 0$ (broken line) is shown for comparison. The inhomogeneous width is 318 cm^{-1}.

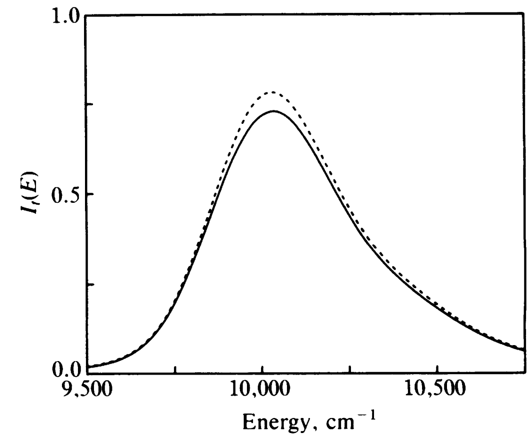

FIG. 5. Photochemically modified absorption (solid line) spectrum for the fully interacting chromophore system. All parameters are as in Fig. 4, except $J_{CT} = 240$ cm^{-1}. The $C = 0$ spectrum (broken line) is shown for comparison.

IMPLICATIONS FOR CHARGE SEPARATION DYNAMICS

In the context of the model described at the beginning of the paper, the above calculations indicate that the accessible excited state manifold in the Q_y energy region consists of eigenstates with substantial admixture of both P* (which carries oscillator strength) and P^+B^- character. The nature of the vibronic coupling Hamiltonian leads to a "chaotic" (as opposed to sharp line) spectrum, much as in high-energy regions of molecules excited in supersonic beams (22) (although the physical mechanism that produces spreading of oscillator strength is quite different here).

The translation of this picture into the time domain is the resonant evolution of primary charge separation described in ref. 2. The initially prepared state is a superposition of P* and P^+B^- levels, which rapidly evolves into a thermally equilibrated distribution among P*, P^+B^-, and P^+BH^-. This provides a simple explanation of the activationless nature and rapidity of the reaction. The low yield of delayed fluorescence from P* is then due to statistical factors (P^+BH^- having a lower energy), while failure to return to the ground state PBH can be attributed to a small medium reorganization energy (i.e., one is in the inverted region). This last feature does not impede the speed of initial charge separation

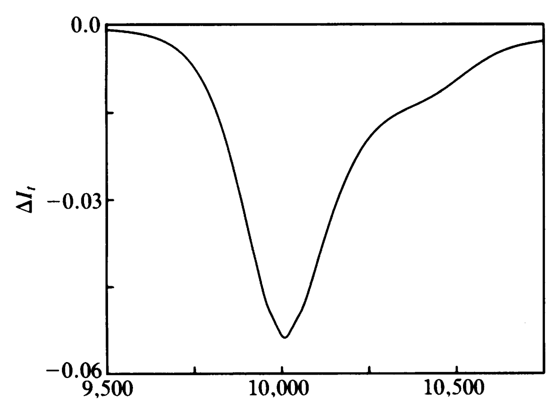

FIG. 6. Hole spectrum $\Delta I_t = I_t - I_{t=0}$ obtained from the corresponding absorption spectra in Fig. 5. The hole width is $\approx$350 cm^{-1}.

(as it would in a typical solution electron transfer reaction) because of the small energy gap and, most importantly, the large exchange matrix element required to explain the hole-burning results.

CONCLUSION

We have shown here (within the limitations of various theoretical approximations) that the hypothesis that the primary donor interacts with a nearly resonant, strongly coupled CT state is sufficient to explain the experimental hole-burning results, while other, less powerful, assumptions (e.g., electrostatic perturbations from distant levels) are insufficient. Furthermore, such a spectrum would not arise from the dimer by itself. An alternative explanation is difficult to conjecture at this point.

We believe that this resonant state participates in the initial charge separation in a manner described quantitatively by the calculations of ref. 2. The precise electronic identity of the state does not affect the validity of either the hole-burning or dynamical calculations, although it may lead to different predictions of parameter values. The latter possibility may be investigated by more detailed simulations.

The vibronically coupled molecular modes ensure that accessible resonant levels exist; without them, a much more precise tuning of the electronic energy gaps would be required. The chaotic spreading of oscillator strength (as opposed to regular vibronic progressions) results from the Born–Oppenheimer breakdown in the multilevel electronic system. Irregular spacings of absorption lines are already apparent in an exciton coupled dimer (23); the CT manifold fills in the gaps, indicating that the full effective Hamiltonian matrix experiences many avoided crossings or level repulsions. The occurrence of this phenomenon (by no means guaranteed, even with a large level density) is a nontrivial result of the theory, achieved by adjustment of one or two parameters.

Assuming that the above picture is correct, our calculations are insensitive to details of the model (e.g., precise values of vibronic coupling parameters). Inclusion of additional electronic or vibrational states would in no way affect the results, as they would serve only to smooth further the broad homogeneous line already generated by the basic model. On the other hand, nonresonant states are by themselves ineffective in producing a large homogeneous hole width, and so cannot explain the experimental results.

One possible experimental test is measurement of the Stark effect in excitation of the 990-nm band. If there is a substantial CT component of those states with oscillator strength [as preliminary experiments suggest (24)], a large effect should be observed. Furthermore, the direction of the difference dipole moment might allow one to distinguish which CT configuration is the principal contributor.

We thank Steve Boxer and his research group for useful discussions. R.A.F. is an Alfred P. Sloan Foundation Fellow and a recipient of a Camille and Henry Dreyfus Teacher-Scholar award. Support from the National Science Foundation is acknowledged.

1. Deisenhofer, J., Epp, O., Miki, K., Huber, R. & Michel, H. (1984) *J. Mol. Biol.* **180**, 385–398.
2. Friesner, R. & Wertheimer, R. (1982) *Proc. Natl. Acad. Sci. USA* **79**, 2138–2142.
3. Boxer, S. G., Lockhart, D. J. & Middendorf, T. R. (1986) *Chem. Phys. Lett.* **123**, 476–482.
4. Boxer, S. G., Middendorf, T. R. & Lockhart, D. J. (1986) *FEBS Lett.* **200**, 237–241.
5. Meech, S. R., Hoff, A. J. & Wiersma, D. A. (1985) *Chem. Phys. Lett.* **121**, 287–292.
6. Völker, S. & Macfarlane, R. M. (1980) *J. Chem. Phys.* **73**, 4476–4482.
7. Scherz, A. & Parson, W. W. (1984) *Biochim. Biophys. Acta* **766**, 666–678.
8. Deisenhofer, J., Michel, H. & Huber, R. (1985) *Trends Biochem. Sci. Pers. Ed.* **10**, 243–248.
9. Martin, J. L., Breton, J., Hoff, A. J., Migus, A. & Antonetti, A. (1986) *Proc. Natl. Acad. Sci. USA* **83**, 957–961.
10. Parson, W. W., Scherz, A. & Warshel, A. (1985) in *Antennas and Reaction Centers of Photosynthetic Bacteria: Structures, Interactions and Dynamics*, ed. Michel-Beyerle, M. E. (Springer, Berlin), pp. 122–130.
11. Shuvalov, A. V. & Parson, W. W. (1981) *Proc. Natl. Acad. Sci. USA* **78**, 957–961.
12. Platenkamp, R. J., Den Blanken, H. J. & Hoff, A. J. (1980) *Chem. Phys. Lett.* **76**, 35–41.
13. Even, U., Magen, J. & Jortner, J. (1982) *Chem. Phys. Lett.* **88**, 131–134.
14. Warshel, A. (1980) *Proc. Natl. Acad. Sci. USA* **77**, 3105–3109.
15. Lagos, R. & Friesner, R. (1984) *J. Chem. Phys.* **81**, 5899–5909.
16. Won, Y., Lagos, R. & Friesner, R. (1986) *J. Chem. Phys.* **84**, 6567–6574.
17. Nauts, A. & Wyatt, R. E. (1983) *Phys. Rev. Lett.* **51**, 2238–2241.
18. Friesner, R., Wyatt, R. E., Hempel, C. & Criner, B. (1986) *J. Comput. Phys.* **64**, 220–229.
19. Gouterman, M. (1961) *J. Mol. Spectrosc.* **6**, 138–163.
20. Breton, J. (1985) in *Antennas and Reaction Centers of Photosynthetic Bacteria: Structures, Interactions and Dynamics*, ed. Michel-Beyerle, M. E. (Springer, Berlin), pp. 109–121.
21. Friedrich, J. & Haarer, D. (1984) *Angew. Chem. Int. Ed. Engl.* **23**, 113–140.
22. Smalley, R. F. (1983) *Annu. Rev. Phys. Chem.* **34**, 129–153.
23. Friesner, R. & Silbey, R. (1981) *J. Chem. Phys.* **74**, 1166–1172.
24. DeLeeuv, D., Malley, M., Butterman, G., Okamura, M. Y. & Fisher, G. (1982) *Biophys. J.* **37**, 111 (abstr.)
25. Boxer, S. G., Gottfried, D. S., Lockhart, D. J. & Middendorf, T. R. (1987) *J. Chem. Phys.* **86**, 2439–2441.